AGU PUBLICATIONS

JGR

Journal of Geophysical Research: Atmospheres

RESEARCH ARTICLE

10.1002/2014JD021846

Key Points:
- Tropopause Inversion Layer (TIL) defined with stability profile diagnostics
- Climatology of TIL diagnostics presented from GPS and reanalysis data
- TIL shows trends over time. Lower Stratosphere "broadening" by 1° per decade

Correspondence to:
A. Gettelman,
andrew@ucar.edu

Citation:
Gettelman, A., and T. Wang (2015), Structural diagnostics of the tropopause inversion layer and its evolution, *J. Geophys. Res. Atmos.*, *120*, doi:10.1002/2014JD021846.

Received 1 APR 2014
Accepted 5 DEC 2014
Accepted article online 9 DEC 2014

Structural diagnostics of the tropopause inversion layer and its evolution

A. Gettelman[1] and T. Wang[2,3]

[1]National Center for Atmospheric Research, Boulder, Colorado, USA, [2]Department of Atmospheric Sciences, Texas A&M University, College Station, Texas, USA, [3]Jet Propulsion Laboratory, California Institute of Technology, Pasadena, California, USA

Abstract The Tropopause Inversion Layer (TIL) is marked by a peak in static stability directly above the tropopause. The TIL is quantitatively defined with new diagnostics using Global Positioning System Radio Occultation temperature soundings and reanalysis data. A climatology of the TIL is developed from reanalysis data (1980–2011) using diagnostics for the position, depth, and strength of the TIL based on the TIL peak in static stability. TIL diagnostics have defined relationships to the synoptic situation in the Upper Troposphere and Lower Stratosphere. The TIL is present nearly all the time. The TIL becomes hard to define in the subtropics where tropical air overlies midlatitude air, in a region of complex static stability profiles. The mean position of the subtropical TIL gradient is sharp and is co-located with the subtropical tropopause break. Over the period 1980–2011 the TIL depth below the tropopause has decreased by 5% per decade and increased above the tropical tropopause by a similar percentage. Furthermore, the latitude of the abrupt change in the TIL from tropical to extratropical in the lower stratosphere appears to have shifted poleward in each hemisphere by ~1° latitude per decade, depending on the diagnostic examined. Reanalysis trends should be treated with caution.

1. Introduction

The tropopause region is characterized by a sharp temperature inversion just above the traditionally defined tropopause [*Wirth*, 2003]. This is easily seen in midlatitudes [*Birner et al.*, 2002] but is present at all latitudes [*Birner*, 2006]. The increase in static stability has been termed the Tropopause Inversion Layer (TIL) and is present in temperature observations from radiosondes [*Birner et al.*, 2002], remotely sensed temperatures from Global Positioning System (GPS) satellites [*Randel et al.*, 2007b] as well as models and analyses [*Birner et al.*, 2006]. The static stability maximum is a consequence of the shape of the thermal profile. The thermal profile is a consequence of radiative [*Randel et al.*, 2007b] and/or dynamical [*Son and Polvani*, 2007; *Grise et al.*, 2010] processes. Static stability is inherently related to the thermal gradients and hence to the dynamic (potential vorticity) definition of the tropopause, reviewed in *Gettelman et al.* [2011].

The TIL is important as (a) a diagnostic of the Upper Troposphere and Lower Stratosphere (UTLS) structures and (b) a barrier or resistance to vertical motion. This work develops a series of diagnostics for the TIL representing the strength (in terms of static stability), depth (in physical space) on either side of the static stability peak, and the relationship of the static stability peak to the tropopause itself, similar to *Schmidt et al.* [2010].

A climatology of the TIL was recently presented by *Grise et al.* [2010] using Global Positioning System (GPS) temperature profile data. *Grise et al.* [2010] found that (a) TIL exists at all latitudes, (b) there are two distinct maxima in the tropics at 17 and 19 km depending on season and latitude, and (c) the TIL structure is closely tied to dynamic variability using 5 day mean anomalies. *Schmidt et al.* [2010] used GPS and in situ temperature profiles to examine the structure of the TIL, identifying a TIL bottom (static stability minimum below the tropopause), TIL maximum (static stability maximum above the tropopause), and TIL top (maximum temperature above the tropopause) and showed that the TIL was "narrower" around the tropopause during summer. *Homeyer et al.* [2010] diagnosed a tropopause transition layer depth with curve fits to static stability profiles and identified the fraction of profiles with canonical TIL structures, as well as highlighting that deep tropopause layer structures are found in conjunction with cyclonic flow (cutoff lows, stratospheric intrusions).

The tropopause region structure has also been used to diagnose changes in the general circulation [*Seidel et al.*, 2008]. Changes in the circulation are expected from the radiative-convective effects of increased

greenhouse gases, which warm the troposphere and cool the stratosphere. The altered thermal gradient in the UTLS in turn affects the subtropical jets (through the thermal wind relationship), tending to increase their speed and alter their position [*Polvani and Kushner*, 2002]. The jets affect the circulation down to the troposphere in a coupled dynamical response that can be diagnosed in the meridional extent of the Hadley circulation [*Held and Hou*, 1980] and the height of the tropopause [*Held*, 1982; *Lorenz and DeWeaver*, 2007]. Observed trends or shifts in the subtropical jet streams or subtropical dry regions can reach 1° latitude per decade but are dependent on the choice of metrics [*Birner*, 2010; *Davis and Rosenlof*, 2012]. *Davis and Birner* [2013] used upper tropospheric metrics for circulation and static stability in reanalysis and GPS data to examine trends in the tropopause region, and many authors have used the tropopause height as a metric for the circulation [e.g., *Lu et al.*, 2009].

This work will examine TIL in high-resolution soundings and in reanalysis data by defining some objective diagnostics of the UTLS stability structure. While the climatology of the TIL structure has been well covered in the literature, here we highlight in the analysis and discussion two distinct sets of questions at either end of the temporal scale. First, how often is the TIL present, how does it relate to the synoptic variability in the UTLS, and what is the climatological and seasonal structure? Second, are there defined trends in the TIL structure that would enable us to diagnose global change and evaluate its representation in global models and analysis systems? The analysis will start from instantaneous and 6-hourly data, and build up to long-term trends. Section 2 describes the diagnostics, data, and methodology. Results are in section 3, and some answers to the questions above are in the discussion (section 4).

2. Methods

TIL statistics are calculated using temperature profiles at each point in space and time, starting with Global Positioning System (GPS) Radio Occultation (RO) temperature measurements with high vertical resolution. Reanalysis temperature profiles can reproduce TIL statistics, and these data are then used to develop a climatology of the structure of the TIL. The seasonal and annual structure is evaluated. Finally, 32 years of reanalysis data are used to examine trends in the TIL.

2.1. Data: GPS, ERA-Interim, and MERRA

GPS RO temperature profile data come from the Constellation Observing System for Meteorology, Ionosphere, and Climate (COSMIC) [*Anthes et al.*, 2008]. Use of the data for the TIL is detailed by *Randel et al.* [2007b] and *Schmidt et al.* [2010]. We use two versions of the GPS data. First are raw profiles from the "wetPrf" data set, produced on a 100 m vertical grid. Vertical resolution of the GPS observations is about 500 m around the tropopause. There are about 1000 profiles per day globally from the COSMIC data in 2011. Second, because we want to average out some of the gravity waves, wetPrf profiles are put on a standard 200 m resolution vertical grid and then binned to daily 1.25° by 1.25° horizontal grid using Gaussian weights. The binning process using different times and coarser vertical resolution smooths out high-frequency waves but maintains the high vertical resolution structure which is a unique feature of the GPS data. Comparisons of individual points indicate that reanalysis (see below) and GPS temperatures for co-located grids differ by less than 0.5 K in the TIL. We analyze 5 years of GPS data (2007–2011).

The gridding of the GPS data is different than previous work [*Randel et al.*, 2007b; *Birner*, 2006], which typically uses raw profiles and then puts them in relative coordinates. Here we are typically averaging and smoothing 1–2 profiles in a day before putting them in relative coordinates. This has the desired effect of removing waves, but preserving tropopause structure (since radiative timescales are long in the UTLS). Previous work with raw GPS data might be actually picking up gravity waves more than TIL structure. We use both methods (raw and gridded) for comparison. We will illustrate that the TIL statistics are essentially the same. There are quantitative differences in the strength metrics between the raw and gridded data, but the structure is the same. The conclusions are not dependent on the use of gridded data as the gridded data have a similar structure for the metrics we are using.

European Centre for Medium Range Weather Forecasts (ECMWF) Interim Reanalysis (ERAI) [*Dee et al.*, 2011] data from 1980 to 2011 (32 years) are used. We use 6 hourly averages of temperature to calculate buoyancy frequency on standard levels and a 1° grid. Vertical resolution of the data is ~1000 m in the UTLS. Statistics described in the next section are calculated from individual grid points in space and time, and averaged. ERAI assimilates the GPS data, so the data sources are not independent.

To understand the sensitivity of the results to the choice of reanalysis data set, we also use the Modern Era Retrospective analysis for Research and Applications (MERRA) [*Rienecker et al.*, 2011]. MERRA is available at 0.5° horizontal resolution, and we also use a version interpolated to 2° grid, both on pressure levels. Vertical resolution is similar to ERAI at ~1000 m in the UTLS. Below we demonstrate that TIL diagnostics are similar between ERAI and MERRA. The same 32 year time period is used for both reanalyses. MERRA does not assimilate GPS observations, providing an independent data set from the GPS data.

2.2. TIL Diagnostics

We will use several diagnostics of the TIL structure, illustrated on GPS stability and temperature profiles in Figure 1. The figure shows equally spaced individual profiles around a latitude circle at the latitude indicated. Static stability is calculated as the squared buoyancy frequency (also called the Brunt–Väisälä frequency):

$$N^2 = \frac{g}{\theta}\frac{\partial\theta}{\partial z} = \frac{g}{T}(\Gamma_d + \Gamma) \quad (1)$$

where Γ is the temperature lapse rate ($\Gamma = \partial T/\partial z$), Γ_d is the dry adiabatic lapse rate, and $g = 9.81$ m s^{-2} the gravitational acceleration. The TIL bottom is defined as the minimum in N^2 in the Upper Troposphere (UT), illustrated by the plus signs in Figures 1a, 1c, and 1e. The TIL peak, or N^2_{max}, is defined by searching for the first maximum N^2 (a change in sign of the vertical gradient of N^2) above a specified threshold (4×10^{-4} s^{-2}) from the TIL bottom, marked by the red triangle in Figures 1a, 1c, and 1e. The position of the TIL peak is analyzed relative to the thermal tropopause, estimated using the standard World Meteorological Organization (WMO) definition [*World Meteorological Organization*, 1957], and shown as the blue square on the temperature profile in the right panels of Figure 1.

The upper bound of the TIL (TIL top) is defined as the minimum in N^2 in the lower stratosphere (LS) above the TIL peak, illustrated by blue diamonds in Figures 1a, 1c, and 1e, and we also note the maximum N^2 in the LS above this (asterix in Figures 1a,1c, and 1e. The maximum N^2 in the LS is sometimes within the TIL and sometimes well above it. This is similar to the vertical structures identified by *Schmidt et al.* [2010] and *Hegglin et al.* [2009].

TIL structure is diagnosed by looking at the gradients on the UT and LS sides of the TIL N^2 peak separately. The UT TIL depth is defined as one half of the distance between the UT N^2 minimum (N^2_{min}) and the TIL peak (N^2_{max}) in distance units (km), and the strength as half ΔN^2 between the UT N^2_{min} and the TIL peak (N^2_{max}) in frequency units (s^{-2}). Half the distance is used to capture the middle of the gradient. The same calculations are performed on the LS side of the TIL peak to generate a LS depth and strength. The diagnostics are summarized in Table 1. Statistics are calculated on each profile and averaged. The diagnostics use distances in coordinates relative to the static stability peak before averaging. This is similar to tropopause relative coordinates used by *Birner et al.* [2002] and others. The methodology for the diagnostics has only two parameters: (a) the bottom threshold in the UT used for finding the UT minimum (500 hPa) and (b) the minimum static stability value allowed for N^2_{max} (4×10^{-4} s^{-2}). We have tested the sensitivity of the results to these parameters. Results are not sensitive to the UT minimum pressure. Reducing the minimum N^2_{max} threshold allows more profiles to be found in the subtropics. This does not affect the climatology, and we have verified it also does not affect trends.

Figure 1 illustrates the variability of stability and temperature in the UTLS in three latitude bands: the tropics (Figure 1a and 1b), the subtropics (Figures 1c and 1d), and the midlatitudes (Figures 1e and 1f) from daily gridded GPS profiles. Raw GPS profiles (not shown) have more scatter, but the diagnostics for the UT have similar structure. In the LS, the raw GPS profiles have large gravity wave temperature perturbations at small vertical scales which complicate the interpretation and diagnosis of the TIL. These variations are largely removed with the gridding process.

There is a different character to the TIL at different latitudes. In the tropics (Figures 1a and 1b), the TIL peak is near 90 hPa, and there is a large stability jump occurring in a narrow layer between the UT and LS. In the subtropics (Figures 1c and 1d), the tropopause is highly variable between 300 and 100 hPa, and the character of the TIL contains some points that look like the tropics, and some that do not, as a consequence of the vertical layering of tropical and extratropical air masses. This is clear in the bimodal distribution of tropopause pressures in Figure 1d. This also gives rise to "double tropopause" structures where a tropical airmass overlies a midlatitude one. In some of these profiles, the method of diagnosing the TIL breaks down (see below). The change in the TIL character is a consequence of sampling tropical and extratropical air at different longitudes in the subtropics. The diagnostics reflect this. Finally, at middle and high latitudes (Figures 1e and 1f),

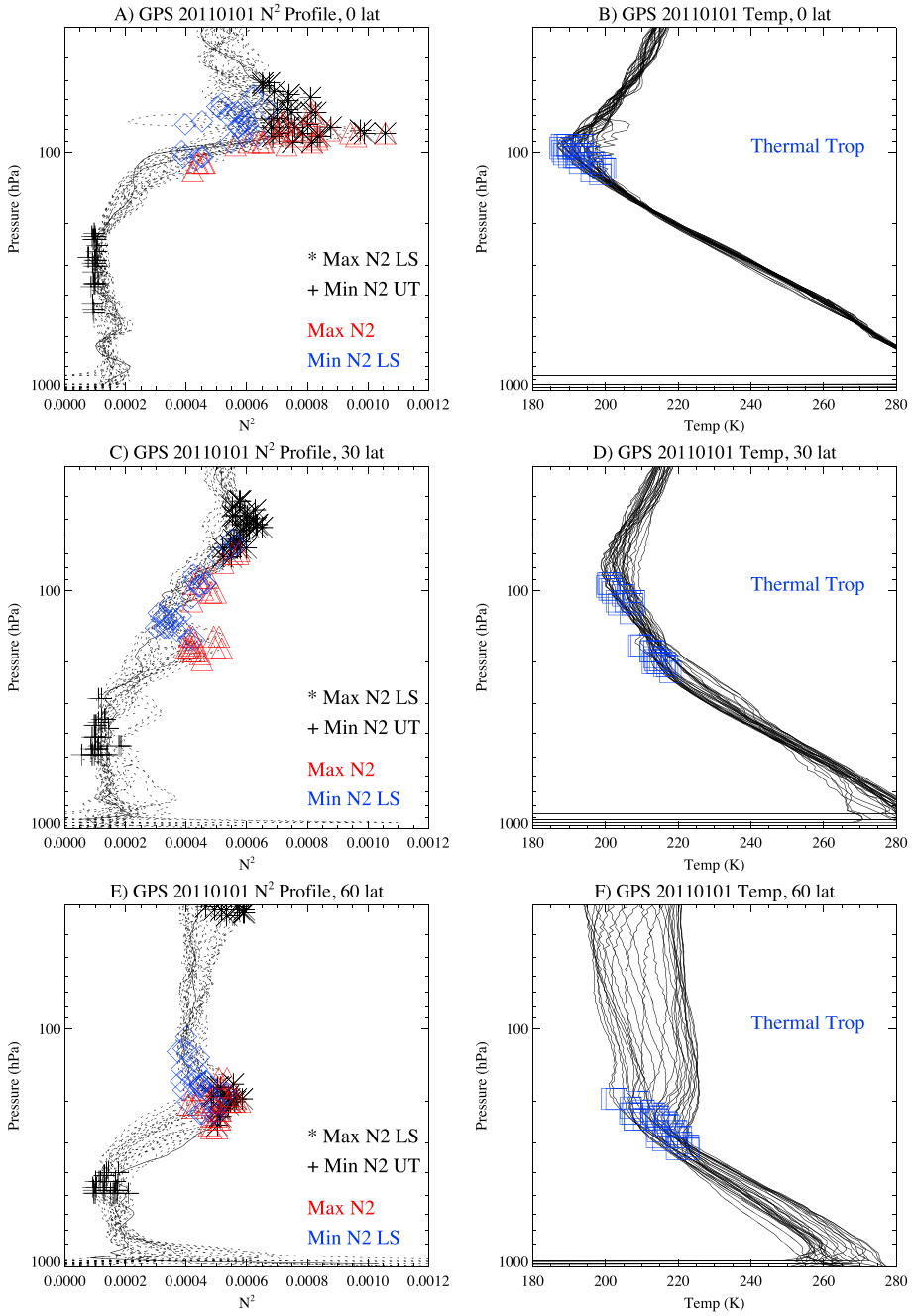

Figure 1. TIL Diagnostics illustrated using gridded GPS Profiles every 10° of longitude on 1 January 2011. (a, c, and e) Stability (N^2) profiles with the UT N^2_{min} (black cross), LS N^2_{max} (black asterix), UT N^2_{max} (red triangle), and LS N^2_{min} (blue diamond). (b, d, and f) Temperature profiles with the thermal tropopause (blue square). Different latitudes shown: (a, b) equator, (c, d) 30°N, and (e, f) 60°N.

the TIL is at a lower altitude, and also highly variable, but with a consistent structure. The ΔN^2 across the TIL is not as large as in the tropics. The stratospheric temperatures vary significantly between profiles (Figure 1f), as does the tropopause temperature and pressure.

We now turn to examining profiles based on reanalysis data. Figure 2 is similar to Figure 1 but for ERAI reanalyses for the same date. As would be expected, the structures are very similar for the ERAI and GPS profiles, and the character by latitude is maintained. This is also expected because the ERAI reanalysis does assimilate the COSMIC GPS. The basic difference between the data sets is the vertical resolution: the GPS

Table 1. Definitions of TIL Diagnostics

TIL Diagnostic	Definition	Units
Frequency	Frequency N^2_{max} is defined	Frequency
N^2_{max} Diff	Distance: N^2_{max} - Tropopause	km
UT Depth	Distance: [h(N^2_{max}) - h(UT N^2_{min})]/2	km
LS Depth	Distance: [h(LS N^2_{min}) - h(N^2_{max})]/2	km
UT Strength	$\Delta N^2 = (N^2_{max}$ - UT $N^2_{min})/2$	s^{-2}
LS Strength	$\Delta N^2 = (N^2_{max}$ - LS $N^2_{min})/2$	s^{-2}

data have higher vertical resolution, which may be critical for the representation of the TIL. *Gettelman et al.* [2010] examined the TIL in global models at different resolutions and found that higher (300 m) and lower (1 km) vertical resolutions were qualitatively similar but had some quantitative differences. We thus expect that there might be

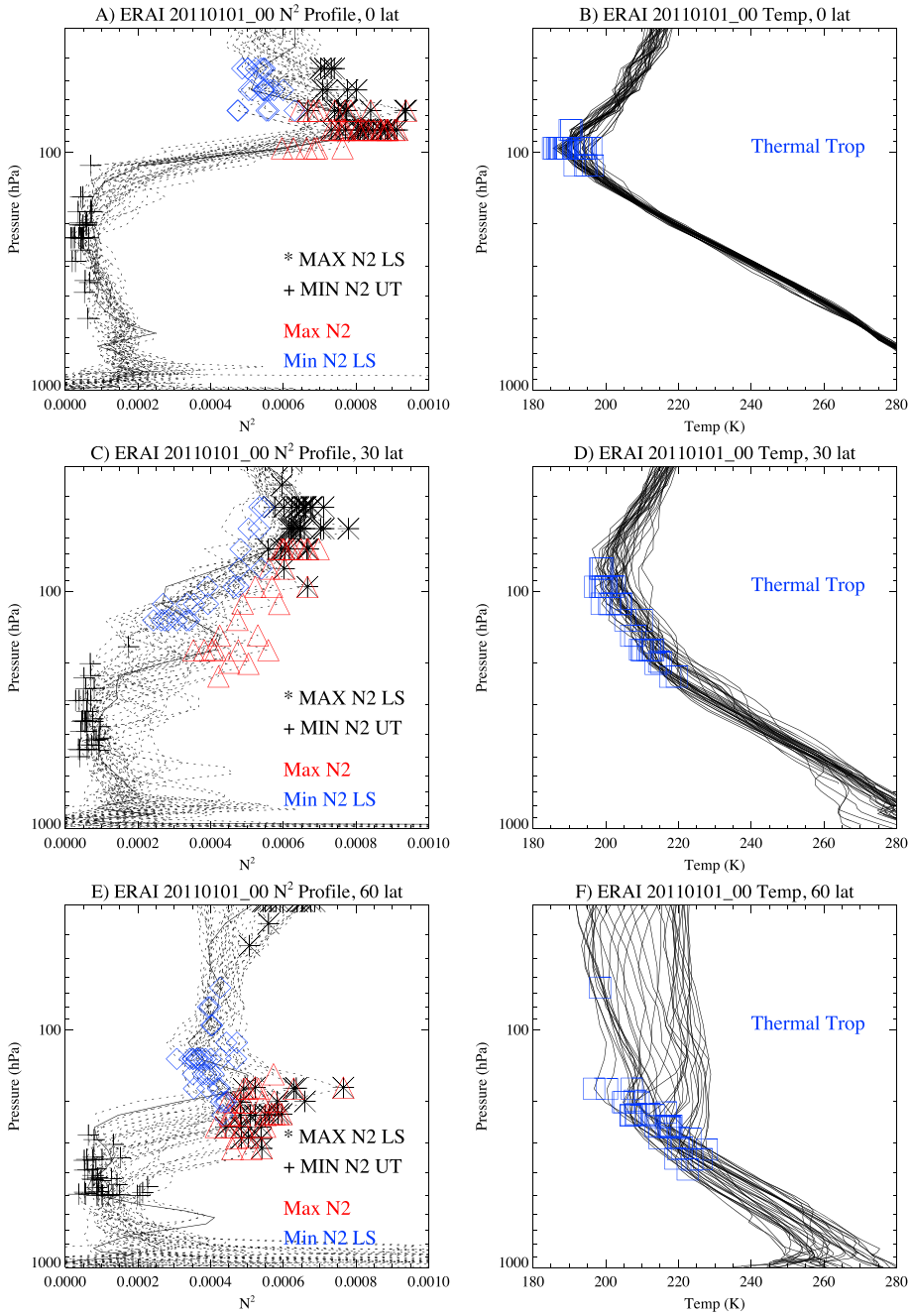

Figure 2. Same as Figure 1 except using ERAI reanalysis for 1 January 2011 at 0 UTC.

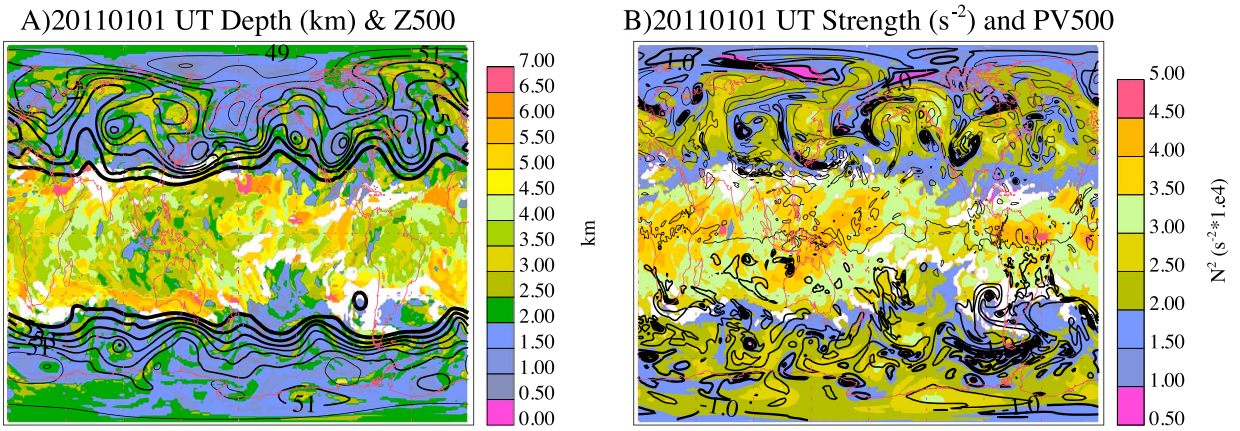

Figure 3. Maps of UT TIL from ERAI data on 1 January 2011 at 0UTC for UT (a) depth (km) and (b) strength (ΔN^2). Overplotted in Figure 3a is the 500 hPa Geopotential (Z500: units of 1000 m^2 s^{-2}) for the same time from ERAI. Thicker contours are higher heights, interval 10^3 $m^2 s^{-2}$. Overplotted in Figure 3b is the 500 hPa Potential Vorticity (PV500), interval 0.5×10^{-6} K m^2 kg^{-1} s^{-1}. White regions indicate where the TIL is not defined.

differences in the strength and depth metrics. In the next section, we will look quantitatively at the daily TIL structure.

3. Results

In this section, the TIL is quantitatively analyzed using the gridded daily GPS and 6-hourly ERAI observations shown in Figures 1 and 2. First, the spatial structure of a snapshot is examined. Then the diagnostics are averaged to monthly and seasonal statistics. Finally, we will extend the record to look at interannual variability and long term trends in the TIL from these diagnostics over the period of the ERAI and MERRA records from 1980 to 2011.

3.1. Instantaneous Structure

The spatial distribution of the TIL diagnostics' variability around a latitude circle shows coherent structures in ERAI data. Figure 3 shows the UT TIL depth (a) and strength (b). Also plotted are (a) 500 hPa geopotential (Z) and (b) Potential Vorticity (PV). Variations of the UT depth diagnostic of the TIL (Figure 3a) are spatially coherent: the depth is high in the tropics and lower in the middle and high latitudes. Depth varies synoptically in high latitudes: UT TIL depth is often large in and adjacent to regions of strong geopotential gradients, which are related to the synoptic variability of cyclonic systems (and the cutoff lows in geopotential) in Figure 3a. Larger UT depth in cyclonic systems is consistent with the expected nature of the static stability profiles in cyclonic systems [*Wirth*, 2003; *Randel et al.*, 2007b]. The maximum UT depth (Figure 3a) occurs in regions of strong geopotential height gradients, both in the subtropics and in the middle and high latitudes associated with cyclonic flow. While the structures and peaks in depth form along geopotential lines, there is not a one-to-one correspondence. There is a distinct band in the subtropics where a TIL peak cannot be defined because there is no clear maximum in N^2. These latitudes correspond to profiles such as that in Figure 2c at 30°N, and represent regions where double tropopause structures are often found in cyclonic features near the subtropical jet [*Randel et al.*, 2007b].

The UT strength diagnostic (Figure 3b) has a similar pattern. There is often a strong anticorrelation between large UT TIL depth and strength, mostly around the edges of synoptic features. This has been verified quantitatively with an anomaly pattern correlation analysis (zonal mean removed) between (a) depth and strength metrics and between (b) the metrics and the 500hPa PV field at different times. Significant pattern correlations result. A shallow (deep) TIL is stronger (weaker). TIL UT strength (Figure 3b) is anticorrelated strongly with PV, consistent with balanced dynamical structures [e.g., *Wirth*, 2000, 2003].

High PV results in lower TIL UT strength, and this is often found in regions where the tropopause is low (in cyclonic systems around low geopotential heights), consistent with *Homeyer et al.* [2010]. *Wirth* [2001] and *Wirth* [2003] also found in an idealized model that latent heating in cyclones erodes stability gradients (and increases PV). High 500 hPa PV is correlated with larger UT TIL depth and lower strength. Higher 500 hPa PV would imply higher midtropospheric static stability and thus a lower gradient to the TIL N^2_{max}.

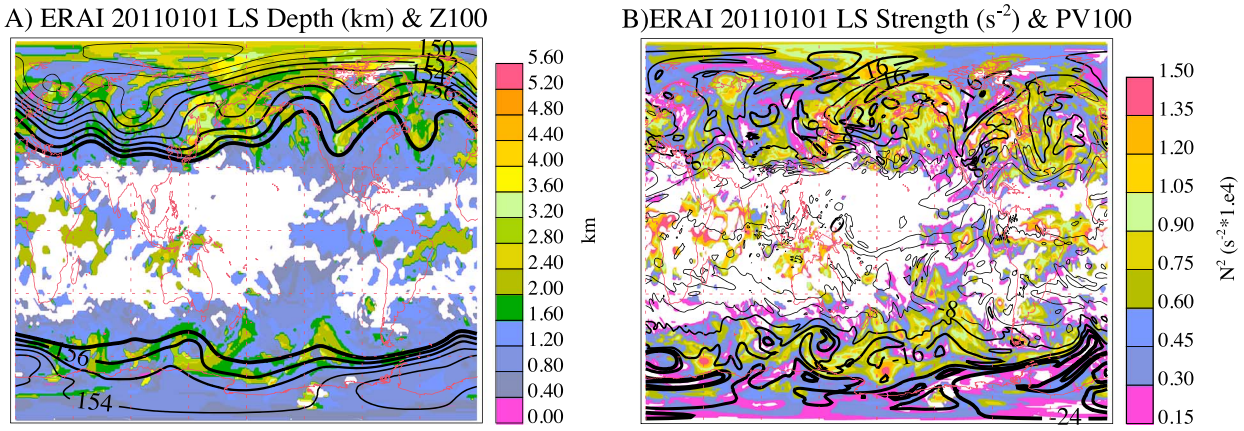

Figure 4. Maps of LS TIL from ERAI data on 1 January 2011 at 0 UTC for LS TIL (a) depth (km) and (b) strength (ΔN^2). Overplotted in Figure 4a is the 100 hPa Geopotential (Z100) for the same time from ERAI. Thicker contours are higher heights, interval 1000 $m^2 s^{-2}$. Overplotted in Figure 4b is the 100 hPa Potential Vorticity (PV100), interval 4×10^{-6} K m^2 kg^{-1} s^{-1}. White regions indicate where the TIL is not defined.

Another way of looking at the correlation is that high PV results from a stretching of the UTLS column and a lower tropopause with an increase of relative vorticity. This would also increase the UT TIL depth and decrease the the N^2_{max}, but not the UT TIL N^2_{min}, thus also reducing UT TIL strength.

The structure of the TIL in the lower stratosphere is illustrated in Figure 4. The LS TIL depth is ill defined in most of the tropics (white regions in Figure 4a), because a N^2 minimum above the tropopause is not clear. The LS TIL depth increases poleward following the synoptic variability of 100 hPa geopotential height (Z100) in Figure 4a, consistent with analysis of the TIL in radiosondes by *Birner* [2006]. The LS TIL strength also is ill defined in the tropics (for the same reasons as LS TIL depth being ill defined). LS TIL strength is positively correlated with LS TIL depth at higher latitudes (based on pattern correlation statistics). LS TIL strength and depth are anti-correlated with the magnitude of 100 hPa PV (PV100) in the Southern Hemisphere, but less clearly in the Northern Hemisphere.

The structure of the height difference between the TIL peak and the tropopause (not shown) is also coherent in space, but with fewer spatial gradients. The basic pattern is clear from the zonal mean (Figure 5b), with the TIL peak within 1 km of the thermal tropopause at high latitudes. There is a band in the subtropics where a maximum in N^2 is not well defined, and around this band, the difference has a much larger separation of 2–3 km. This structure is also clear in *Schmidt et al.* [2010, Figure 9]. In the extratropical latitudes, higher 500 hPa PV is found in regions with lower UT TIL strength (Figure 3b). This is not surprising dynamically, given that PV $\propto$ N^2 [*Gettelman et al.*, 2011], which is in turn related to pressure gradients and baroclinic structures represented in the Geopotential. This relationship between PV and N^2 ties the TIL to PV structures, as stability is the vertical component of PV.

Figure 5 shows the instantaneous zonal mean structure of the TIL diagnosed from 6-hourly ERA interim reanalysis at the same time as the maps in Figures 3 and 4. Figure 5a illustrates the frequency of the locations around a latitude circle where the TIL N^2_{max} can be defined. This has two clear minima, near regions where the stability structure is not sharp, around 40°S (summer) and 30°N (winter). Profiles of the TIL in the subtropics correspond to Figures 2c and 2d from the reanalysis data and Figures 1c and 1d from GPS data. These locations mark the position of the subtropical tropopause "break," where the temperature profile has broadly increasing stability, but sometimes no clear maximum. Hence, these are the same regions where the distance between the TIL peak and the tropopause is large (Figure 5b), similar to results of *Schmidt et al.* [2010]. Consequently, the UT depth of the TIL is also large in these latitude bands (Figure 5c), peaking where the N^2_{max} distance to the tropopause (Figure 5b) is larger but a bit more equatorward than where the TIL becomes indistinct (Figure 5a). The UT TIL depth in the extratropics seems broadly constant with latitude. Figure 5d shows the UT TIL strength. There is a clear separation between the tropics and the extratropics. Figure 5e shows the LS depth of the TIL, which has less distinct minima in depth in the subtropics, as does the LS stability gradient strength (Figure 5f).

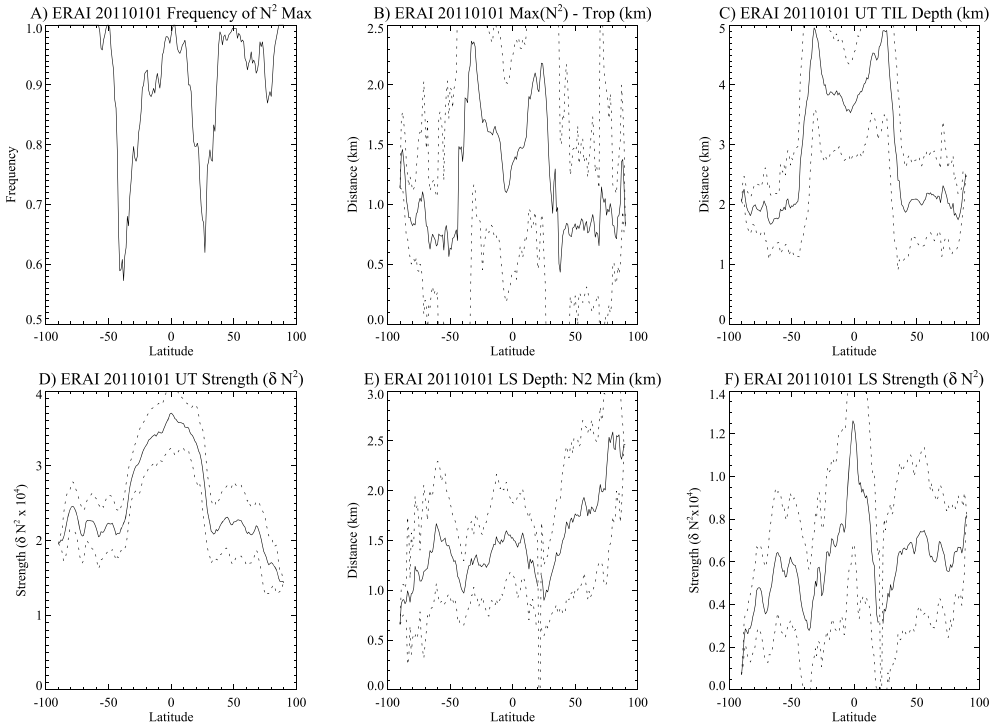

Figure 5. Zonal Mean TIL Diagnostics from ERAI reanalysis. (a) Frequency that N^2_{max} can be defined, (b) relationship of the TIL peak (N^2_{max}) to the tropopause, (c) UT TIL depth (km), (d) UT TIL strength (ΔN^2), (e) LS TIL depth (km), and (f) LS TIL strength (ΔN^2). Dotted lines are the standard deviation around a latitude circle.

The TIL diagnostics developed here from ERAI reanalysis temperature profiles are consistent with previous work using radiosondes and GPS occultation temperature profiles. The diagnostics are synoptically coherent in space with a broader and weaker TIL associated with cyclonic systems. ERAI is able to represent these metrics of the TIL. This was not the case for analysis of the NCEP/NCAR reanalysis by *Birner et al.* [2006], though different metrics were used. The TIL has sharp gradients in the separation of the N^2_{max} from the tropopause, and in particular the depth of the LS and UT sides of the TIL. This single snapshot is consistent with previous work on climatologies of the TIL [*Grise et al.*, 2010; *Schmidt et al.*, 2010].

3.2. Monthly Mean

We now turn to look at the monthly mean and quantitatively compare GPS and ERAI data. Figure 6 illustrates a January monthly mean of the diagnostics from Figure 5. We have also analyzed other months and the differences between data sets are consistent (e.g., in July, the comments about winter and summer hemispheres still hold). Averages of four different data sets are shown in the figure: (1) ERAI data in black, (2) gridded GPS data (vertical resolution 200 m) in red, (3) individual raw (100 m vertical resolution) GPS profiles in blue, and (4) MERRA reanalysis at 0.5° (purple) and 2° (green) horizontal resolution. For comparison, the GPS data have been smoothed with a 1 km boxcar smoother to better capture a similar resolution: but the results are not that sensitive to the smoother. The dotted lines are the standard deviation of the ERAI monthly means around a latitude circle. The dashed lines are the mean of the ERAI standard deviation over time at each longitude around a latitude circle. The latter is usually larger. Averages are taken over all available profiles. The frequency of occurrence is at least 60% at all latitudes (Figure 6a) and is higher in July (at least 80%).

The coarse vertical resolution of the ERAI and MERRA analysis means that finding an appropriate N^2_{max} in the tropopause region tends to fail in the subtropics (Figure 6a) between 10% and 30% of the time. Better vertical resolution means that the definition almost never fails for gridded GPS data (Figure 6A red) and does not fail at all for raw GPS profiles. In fact, the raw GPS profiles have the the opposite problem of too much variability. Specifically, the raw GPS data in the lower stratosphere have significant short vertical wavelength (< 1 km) gravity wave variance, which makes the TIL LS definitions hard to establish. Some of the variance is also measurement noise [*Marquardt and Healy*, 2005]. So these data are not analyzed in Figures 6e and 6f.

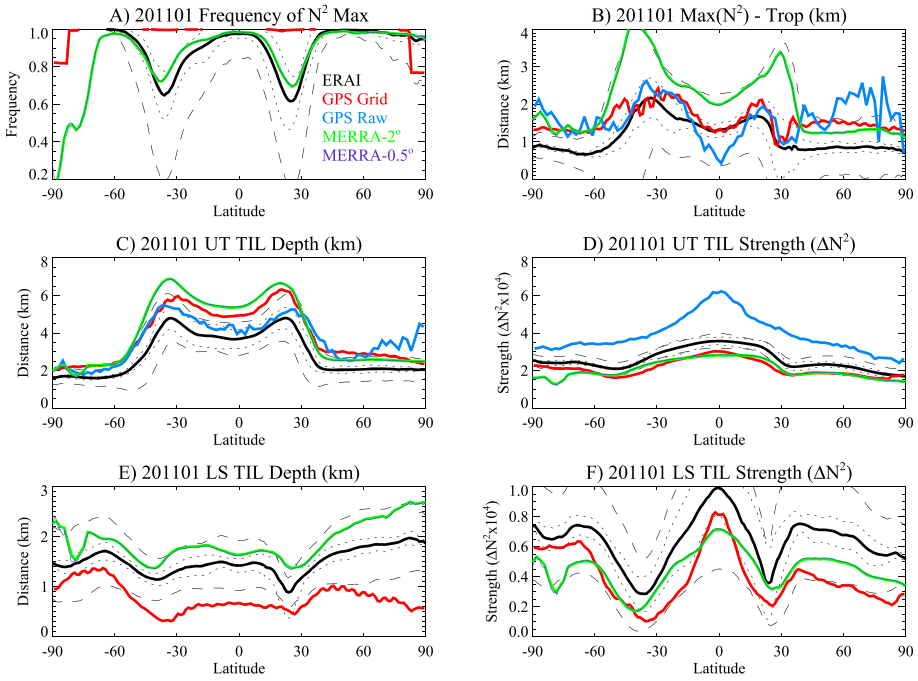

Figure 6. Monthly zonal mean TIL diagnostics from ERAI (black), gridded GPS (red), raw GPS (blue), MERRA 2° (green), and MERRA 0.5° (purple) data. Dotted lines are the ERAI standard deviation of the monthly means around a latitude circle. Dashed lines are the mean of the ERAI individual longitude location standard deviations. Diagnostics are (a) frequency that a N^2_{max} can be defined, (b) relationship of the TIL peak (N^2_{max}) to the tropopause, (c) UT TIL depth (km), (d) UT TIL strength (ΔN^2), (e) LS TIL depth (km), and (f) LS TIL strength (ΔN^2).

Figure 6b shows the separation between the TIL peak (N^2_{max}) and the tropopause. There are distinct peaks in the monthly means from all four data sets, and these occur very close to the same latitude. The GPS data only features about 1000 profiles a day, perhaps a few hundred in a month in a given latitude band, so the data are noisier than the ERAI analysis and have a larger standard deviation which encompasses the ERAI data. The key feature is that the quantitative value of the separation is similar at the subtropical peak (about 2 km), and the latitude of the peak distance in the subtropics is similar across data sets. We have analyzed a longer term GPS climatology (2007–2011), and results are similar. They are also similar to *Schmidt et al.* [2010, Figure 9].

The similarity across the data sets is also high for the UT TIL depth (Figure 6c). The correspondence between data sets is not surprising as gridded GPS and ERAI are dependent on the raw GPS profiles (gridded for the gridded GPS data and assimilated into ERAI). Thus, it is not an independent validation: the comparisons are designed to show that using the reanalysis data yields similar results to the raw higher resolution data, but with better statistics. The differences between the raw GPS (Figure 6c, blue) and the gridded GPS (Figure 6c, red) are largest in the winter hemisphere tropics and high latitudes (also true in July). The difference may be a result of gravity wave activity removed from the gridded profiles. The difference between gridded and raw profiles may also be because the static stability is lower in the stratosphere in polar regions in winter [*Wirth*, 2001], making the TIL broader and harder to define.

The effects of vertical resolution are seen in the UT strength (Figure 6d) and the LS TIL depth (Figure 6e) and strength (Figure 6f). For UT strength, the raw GPS profiles and gridded profiles differ significantly. For the lower stratosphere, the effect is the opposite: the LS TIL depth is shallower (Figure 6e) with a lower LS TIL strength (Figure 6f).

Thus, ERAI data represent the TIL diagnostics from GPS soundings, whether gridded or not. The meridional and spatial (see below) structure of the TIL diagnostics is similar across all the data sets: the meridional gradients shown in Figures 6a–6d are the same between the different ways of using the GPS sounding data. All three data sets are dependent on GPS soundings, generally considered to be an accurate representation of the tropopause region thermal structure.

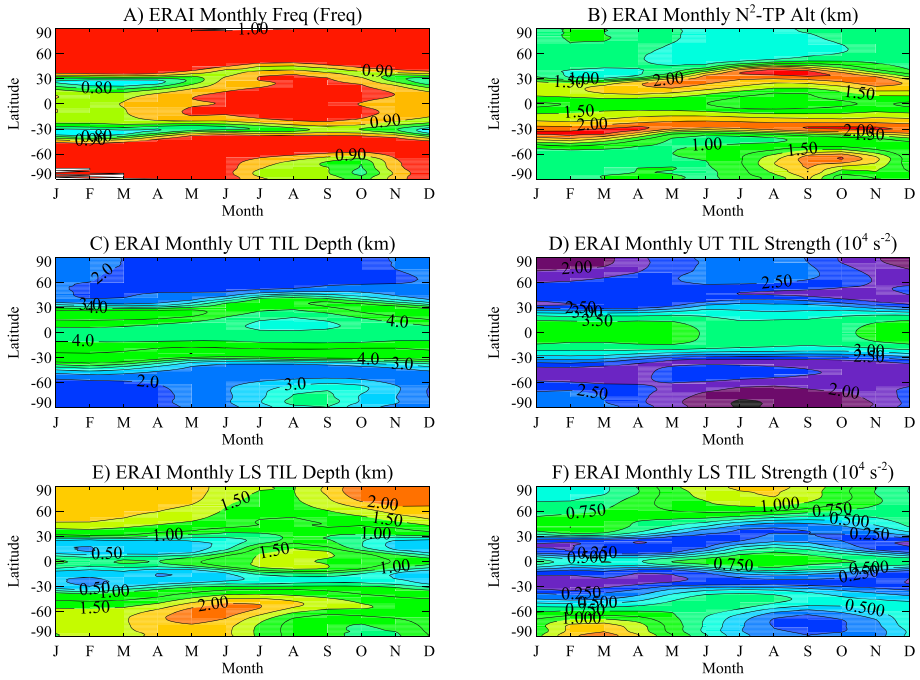

Figure 7. Annual Cycle climatology from 32 years of ERAI data. Diagnostics are (a) N^2_{max} frequency (contour interval 0.05), (b) distance of the TIL peak (N^2_{max}) to the tropopause (contour interval 0.5 km), (c) UT TIL depth (contour interval 0.5 km), (d) UT TIL strength (contour interval $0.5 \times 10^{-4} s^{-2}$), (e) LS TIL depth (contour interval 0.5 km), and (f) LS TIL strength (contour interval $0.5 \times 10^{-4} s^{-2}$).

We have also analyzed MERRA reanalysis data in Figure 6 at 0.5° (thin purple) and 2° (green) resolution. The resolution does not matter (the 2° data are interpolated from the original 0.5° reanalysis) for the TIL diagnostics. Qualitative structure is similar to ERAI, but there are some quantitative differences, mostly due to the positioning of the tropopause (Figure 6b) and at high latitudes of the Southern Hemisphere, where there are some anomalies in interpolation to pressure levels from model levels around Antarctica. In summary, the TIL diagnostics provide meaningful information and robust structure in the UTLS region. The spatial structure of the monthly mean TIL diagnostics is basically identical between the gridded GPS, ERAI, and MERRA data for all the diagnostics. There are quantitative differences between data sets. ERAI is closer to gridded or GPS data for the N^2_{max}—tropopause difference (Figure 6b) in the subtropics than MERRA. MERRA seems to represent the UT depth (Figure 6c) and strength (Figure 6d) better than ERAI relative to the gridded GPS data. LS TIL depth (Figure 6e) is the most sensitive to data differences.

3.3. Annual Cycle

Having demonstrated that the reanalysis is producing similar results to the GPS profiles themselves (which we have taken as the reference data, and on which the reanalysis is partially dependent for input data), we now use the long term record from ERAI reanalysis to diagnose the climatology of the TIL seasonally and over the annual cycle.

Figure 7 shows climatological seasonal means based on 32 years of ERAI analyses of the TIL. For most of the diagnostics, there is a clear seasonal cycle to the TIL. The annual cycle analyzed with MERRA reanalysis looks qualitatively similar, with some quantitative differences as seen in Figure 6. We have also looked at the annual cycle from 5 years of GPS gridded profiles (not shown). The annual cycle in gridded GPS data is similar to that noted below. There are quantitative differences between ERAI and gridded GPS data for UT TIL depth (Figure 6c) and LS TIL depth (Figure 6e) that carry through to the annual cycle. The frequency of TIL definition in the ERAI data is mostly an artifact of the coarse vertical resolution, but it has a consistent cycle, with lower values in the subtropics from December to May and then higher frequencies from June to November (Figure 7a). The lower frequencies in December to May are consistent with the annual cycle of double tropopause events [*Randel et al.*, 2007a]. The frequency minimum in the subtropics shifts poleward in the summer hemisphere, but it is more pronounced in the Northern Hemisphere. The reduced

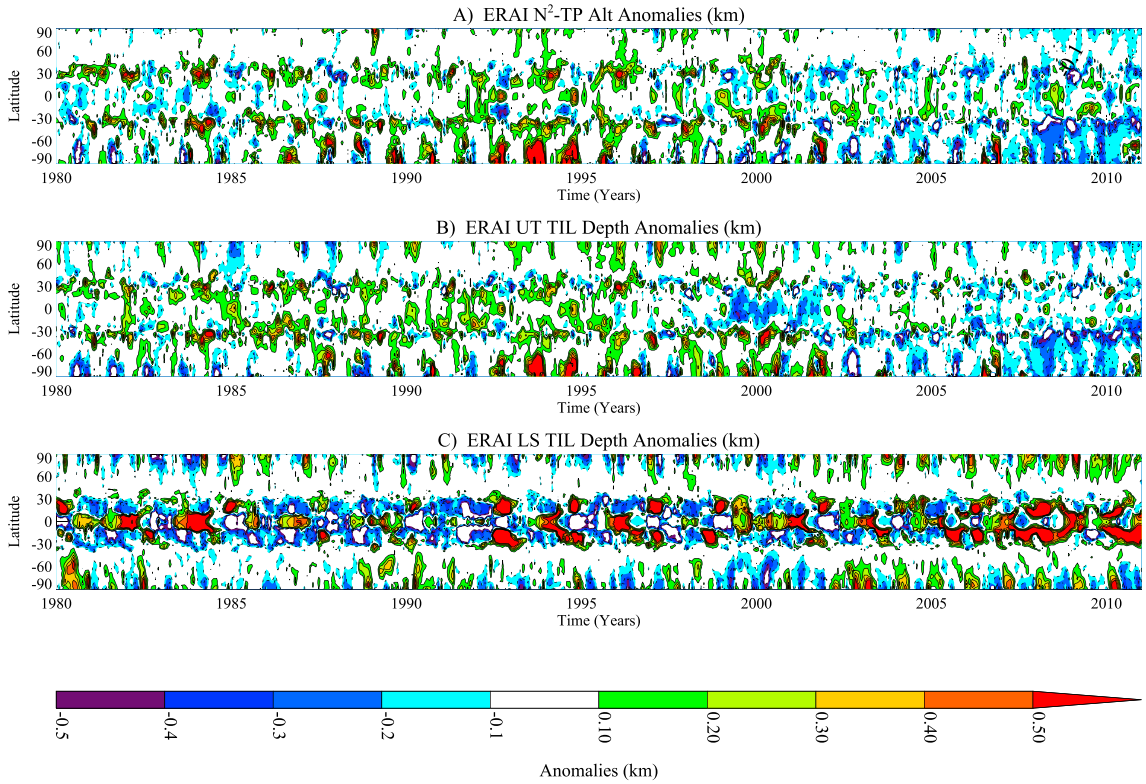

Figure 8. Zonal mean anomalies of TIL diagnostics over time. (a) Relationship of the TIL peak (N^2_{max}) to the tropopause (km), (b) UT depth of the TIL (km), and (c) LS depth of the TIL (km).

frequency in winter and spring at high latitudes of the Southern Hemisphere is likely due to the definition of the thermal tropopause and TIL in this season [*Randel and Wu*, 2010].

The separation of the N^2_{max} and the tropopause (Figure 7b) also has a clear cycle with more variation in the Southern Hemisphere, and again, with the summer hemisphere subtropical peak being further poleward in both hemispheres. The TIL UT depth (Figure 7c) also shifts poleward in the summer hemisphere, and the depth in the extratropics is larger in the winter hemisphere, with a larger annual cycle in the Southern Hemisphere consistent with GPS climatologies [*Schmidt et al.*, 2010; *Grise et al.*, 2010]. The UT TIL strength (Figure 7d) is stronger in the tropics in Northern Hemisphere winter and spring (also seen in *Grise et al.* [2010]). In the extratropics, the strength is lower than in the tropics (consistent with the static stability profiles seen in Figures 2 and 1). There is a strong seasonal cycle, with the strength at high latitudes stronger in the summer season. This cycle is consistent with a combination of effects: in the tropics, it is likely that the annual cycle of tropical tropopause temperatures due to the stratospheric residual circulation dominates the annual cycle in static stability. In the extratropics, the strongest, narrowest, and sharpest TIL is found during polar summer, consistent with *Birner* [2006] and *Randel and Wu* [2010].

In the lower stratosphere (Figures 7e and 7f), the TIL has a reduced depth in the subtropics. The reduced depth in the LS is likely a consequence of the increased depth on the tropospheric side combined with the double peaked vertical structure of subtropical TIL with higher static stability at 19 km [*Grise et al.*, 2010]. There is a broad subtropical minimum in depth and strength, with higher values in Northern Hemisphere summer. The LS depth is largest in the Southern Hemisphere in fall (MAM) and smallest in spring (SON) (Figure 7e), mirrored in the Northern Hemisphere. The TIL has a smaller depth (Figure 7e) but increased strength (Figure 7f) in Northern Hemisphere summer. There is more coherence with the LS TIL strength (Figure 7f), with high latitude maxima in strength in the summer and fall in both hemispheres: consistent with radiative effects of water vapor at high latitudes [*Randel and Wu*, 2010]. The depths between the UT (Figure 7c) and LS (Figure 7e) are broadly anticorrelated in the subtropics and tropics. The annual cycle of UT (Figure 7d) and LS (Figure 7f) TIL strength is positively correlated in the extratropics but negatively correlated in the tropics and subtropics.

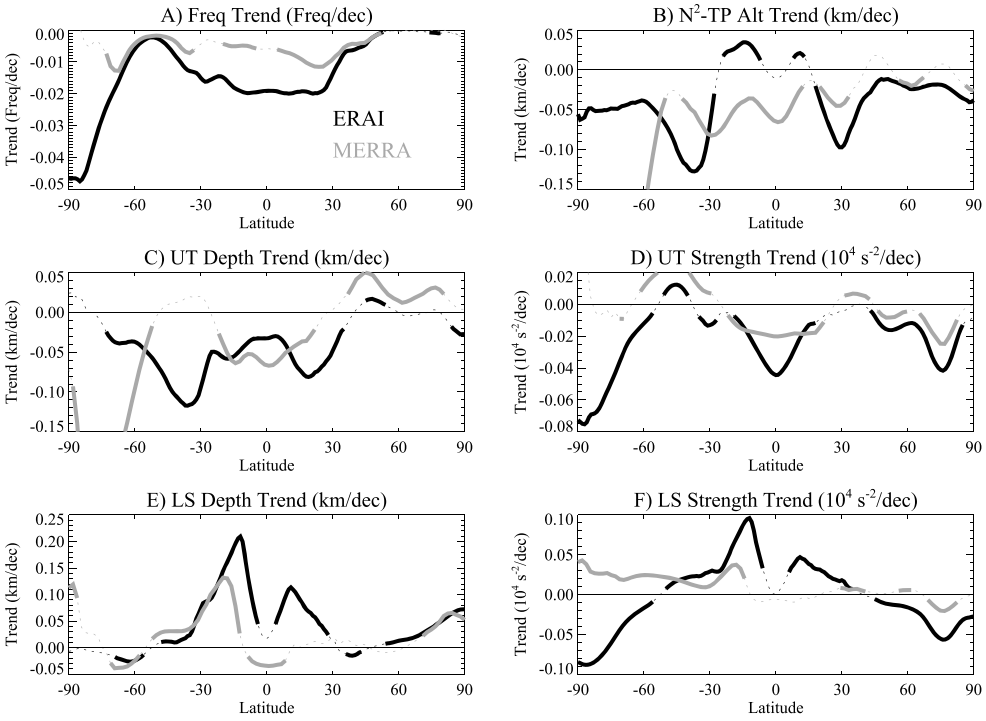

Figure 9. Zonal mean trends for TIL diagnostics over 1980–2011. All trends are per decade. Thick solid line indicates statistically significant trends at the 95% level based on 2σ from a bootstrap fit. ERAI in black, MERRA in gray. (a) Frequency that N^2 max can be defined (km/decade). (b) Distance of the TIL peak (N^2_{max}) to the tropopause (km/decade), (c) UT TIL depth (km/decade), (d) UT TIL strength (10^{-4} s^{-2}/decade), (e) LS TIL depth (km/decade), and (f) LS TIL strength (10^{-4} s^{-2}/decade).

3.4. Interannual Variability

In addition to a climatology based on a long record, the 32 years of reanalysis data allow us to look at the interannual variability and possible secular trends in the structure of the TIL. We will focus on a few diagnostics which seem the easiest to define and have sharp gradients in the subtropics. These are (a) the separation between the TIL peak and the tropopause, (b) the UT TIL depth (representing the upper tropospheric TIL), and (c) the LS depth of the TIL (representing the LS structure). It is important to look at both sides of the TIL, and perhaps separately: the transition from greenhouse gas warming to cooling occurs right around the tropopause, and as greenhouse gases increase over this period, the forcing may cause differential temperature changes and thus changes to TIL structure.

Figure 8 shows monthly mean ERAI anomalies from the annual cycle in Figure 7 for the distance of the TIL peak (N^2_{max}) to the tropopause (Figure 8a), UT TIL depth (Figure 8b), and the LS TIL depth (Figure 8c). The UT TIL peak and UT TIL depth (Figures 8a and 8b) anomalies get more negative over time, particularly at high southern latitudes. Deviations over time are positive in the subtropics early in the record, and in the 21st century are largely negative, again, indicating a "thinning" or "sharpening" of the TIL over time. Trends in LS TIL depth (Figure 8c) are less clear. As noted, ERAI assimilates GPS data from 2006 to 2012, so any trends should not be evident as a "jump" after 2006. We investigate these trends further by looking at them more quantitatively. Anomalies from MERRA reanalysis which does not assimilate GPS data (not shown) indicate a similar anomaly structure, especially the anomalies in the Southern Hemisphere in the 21st century from 2008 to 2012 in Figure 8. This indicates some robustness to the trends, and that these anomalies are not a consequence of using recent GPS data as input in ERAI.

3.5. Trends

Figure 9 shows zonal mean linear trends in the TIL diagnostics derived from ERAI (black) and MERRA (gray). Linear trends are calculated at each latitude with a bootstrap fit with 500 resamples, which minimizes the effects of the end points of the time series (because it samples different sets of data points when resampling) and provides a confidence interval (standard deviation) on the trend. Figure 9 shows a thick solid line

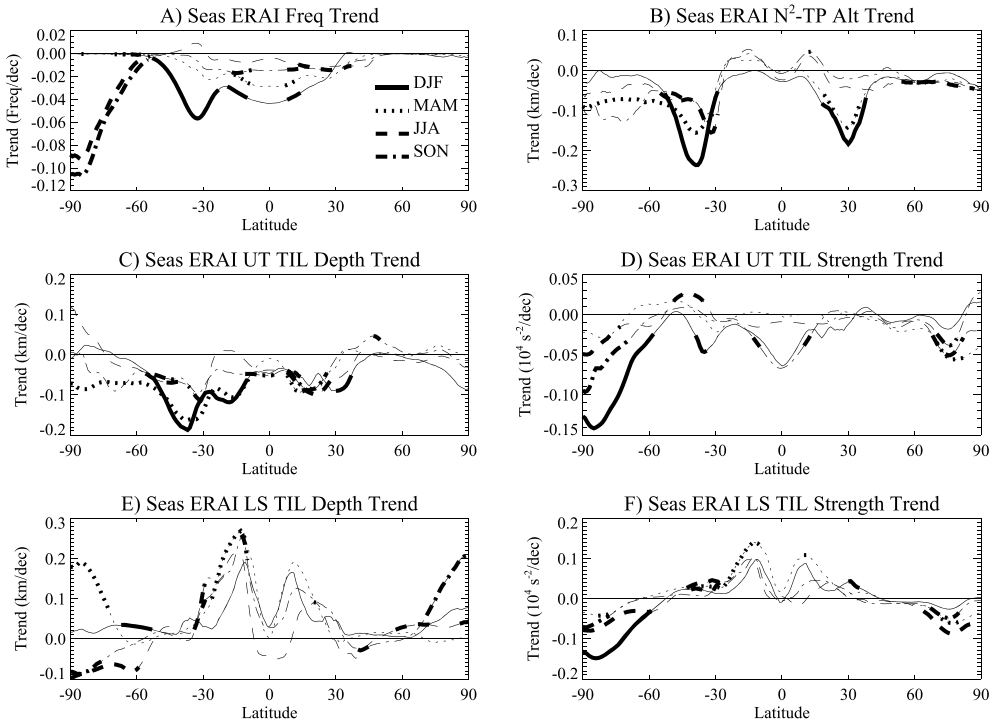

Figure 10. Zonal mean seasonal trends for ERAI TIL diagnostics over 1980–2011. All trends are per decade. Thick solid line indicates statistically significant trends at the 95% level based on 2σ from a bootstrap fit. Seasons are as follows: December to February (DJF: solid), March to May (MAM: dotted), June to August (JJA: dashed), and September to November (SON: dash-dotted). (a) Frequency that N^2 max can be defined (km/decade). (b) Distance of the TIL peak (N^2_{max}) to the tropopause (km/decade), (c) UT TIL depth (km/decade), (d) UT TIL strength (10^{-4} s^{-2}/decade), (e) LS TIL depth (km/decade), and (f) LS TIL strength (10^{-4} s^{-2}/decade).

for trends significant at the 95% (2σ) level. Both ERAI and MERRA (2°) results are shown. There are differences in some of the quantitative results, but especially for the depth and strength trends (Figures 9c–9f), the structure of the trends in sign and magnitude by latitude is similar, indicating limited sensitivity to the reanalysis data used.

The frequency of which the TIL is defined (based on finding a N^2_{max} in the UTLS region) is decreasing slightly in ERAI and MERRA (Figure 9a). This occurs in most seasons (Figure 10a), with slightly larger trends in DJF. The negative trend in frequency may be associated with LS TIL getting deeper (Figure 10e) and thus harder to define. Or a shallower UT TIL (Figure 10c) may become more difficult to resolve with low resolution data, but these trends are only a few percent of the total depth, so this effect is likely small.

The difference in altitude between the N^2_{max} and the tropopause is increasing in the tropics and decreasing at high latitudes in ERAI (Figure 9b). In MERRA, it declines at all latitudes. Largest decreases are at about 30°N and 40°S. In the Northern Hemisphere, this occurs mostly in Winter and Spring (December to May, Figure 10b) and in the Southern Hemisphere, in most seasons (with DJF strongest). Note that the peak trends are just poleward of the seasonal peak separation (Figure 7b). This indicates a meridional shift in the structure of the TIL that we will discuss below.

The depth of the UT TIL (Figure 9c) is decreasing slightly in the tropics and midlatitudes, while there are mostly decreases in UT TIL strength (Figure 9d). The changes are consistent across most seasons (Figures 10c and 10d). There are peaks in the trends for N^2_{max} separation from the tropopause (Figure 9b), UT depth (Figure 9c), and LS depth (Figure 9e) right around the peak values, and so this might be a shift in the structure of the TIL with latitude. The LS TIL depth and strength (Figures 9e and 9f) are increasing in the tropics on the equatorward edges of the peaks in LS TIL depth and strength (Figures 7e and 7f), and there are decreases in strength in the extratropics. This occurs in most seasons (Figures 10e and 10f). The Extratropical TIL is getting slightly thinner (−0.05 km/decade in the extratropics is about 5% per decade), while in the tropics, the depth is increasing in the LS. TIL strength is decreasing at higher latitudes in the UT and LS by a

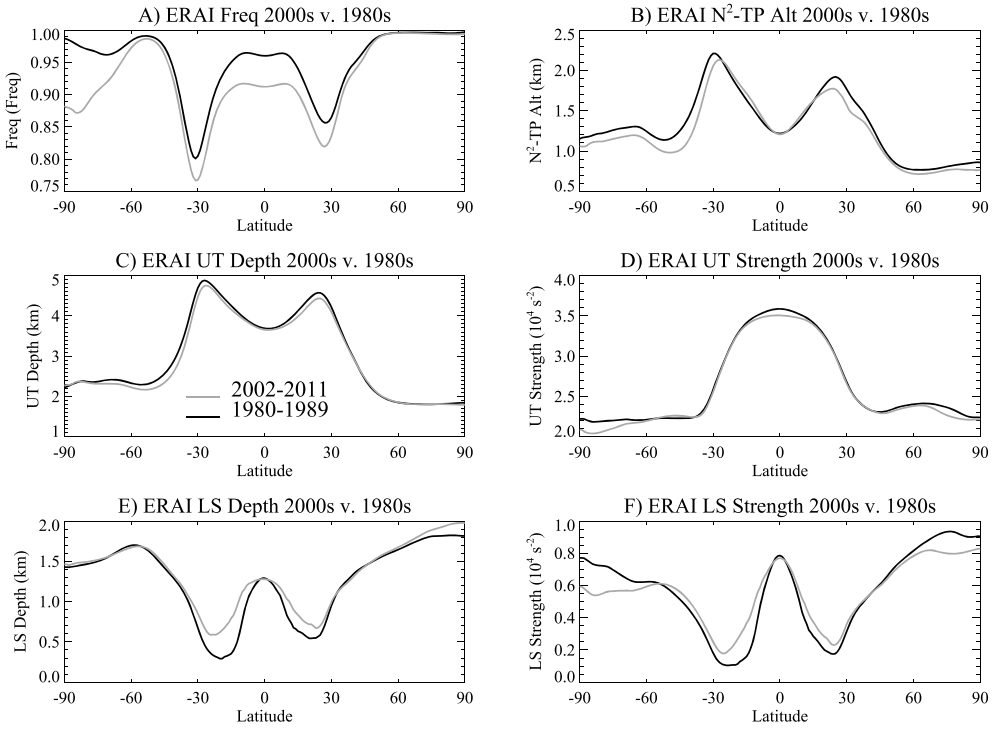

Figure 11. ERAI Zonal mean decadal TIL diagnostics for 1980–1989 (black) and 2002–2011 (gray). (a) Frequency that N^2 max can be defined (freq/decade). (b) Distance of the TIL peak (N^2_{max}) to the tropopause (km/decade), (c) UT TIL depth (km/decade), (D) UT TIL strength (10^{-4} s^{-2}/decade), (E) LS TIL depth (km/decade), and (F) LS TIL strength (10^{-4} s^{-2}/decade).

few percent per decade, up to 10% per decade in the LS (Figure 10f). In the tropical LS, strength is increasing by 10% per decade.

As noted above, there are some important differences between the MERRA and ERAI trends in Figure 9. This suggests significant uncertainty in the estimation of trends from the reanalyses. A healthy skepticism of reanalysis trends is warranted. We have tested the sensitivity to the two "parameters" in the definition and found that the trends are not sensitive to where we start searching for the UT N^2_{min} (600–400 hPa). The choice of a minimum threshold for the N^2_{max} does affect the frequency of definition of the TIL in the subtropics, but we have analyzed the data with thresholds from 3×10^{-4} to 4×10^{-4} s^{-2} and found no change in trends: the error bars all overlap.

Certain common trends stand out. One is the frequency of N^2_{max} in the subtropics (Figure 9a). A second is the extratropical structure of the Northern Hemisphere N^2_{max} separation from the tropopause (Figure 9b), and a third is the change in sign of the trends in UT depth between tropics and extratropics in the Northern Hemisphere (Figure 9c). Note that MERRA trends suffer in the Southern Hemisphere from an issue with trying to readjust for surface pressure around Antarctica. UT strength trends are similar (Figure 9d), as are LS depth trends (Figure 9e).

Trends observed in ERAI data for the separation of N^2_{max} from the tropopause (Figure 9b) and TIL UT depth (Figure 9c) imply a shift in the climatological patterns from the peaks of these values (Figures 7b and 7c). These trends can be viewed as a shift in the subtropical tropopause break where the structure of the UTLS changes from tropical (TTL) to extratropical (ExTL). Another way of looking at the trends is to take composites of the first (1980–1989) and last (2002–2011) decade from the reanalysis records to look at differences between the periods, as in Figure 11. Figure 11 highlights the trends as well as the climatological zonal mean distribution, to enable an understanding of any climatological shifts.

Figure 11 indicates several shifts over time. The N^2_{max} frequency of definition (Figure 11a) is decreasing in the subtropics, and spreading slightly equatorward in each hemisphere. The N^2_{max} peak separation from the tropopause (Figure 11b) is moving slightly equatorward. The UT TIL depth and strength is not changing very

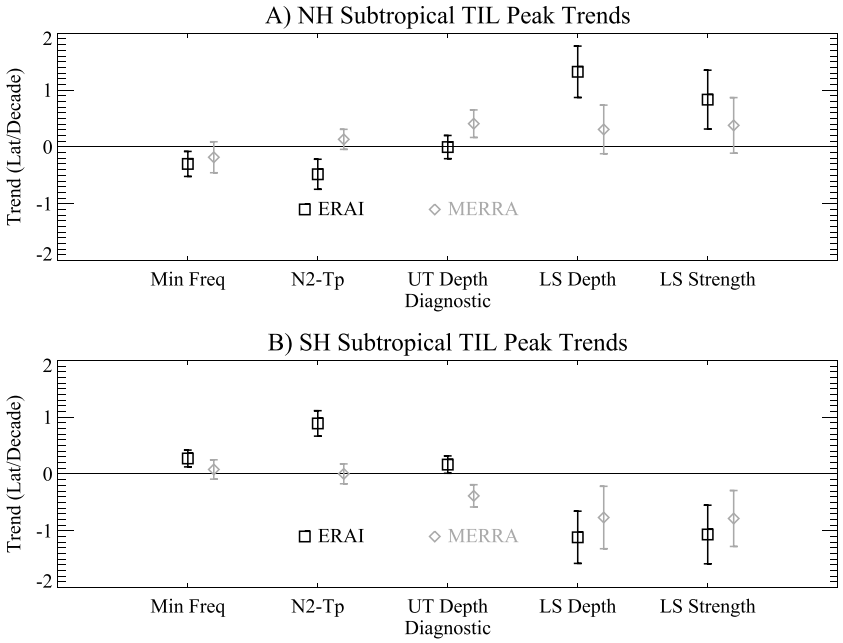

Figure 12. Trends in the subtropical peak latitude for TIL diagnostics for the (a) Northern and (b) Southern Hemispheres. The peak subtropical latitude in the zonal mean for each month is determined, then the annual cycle is removed, and monthly anomalies are calculated. Trends are estimated with a bootstrap method using 500 resamples. Error bars are the 2σ (95%) confidence intervals from the bootstrap trend estimate.

much (Figures 11c and 11d). There is an increase in subtropical LS depth and strength with peaks moving poleward (Figures 11e and 11f).

We investigate this further by finding the peak latitude in the diagnostics for each month and season over the 32 year record and look at the changes in this latitude peak in each hemisphere. Changes in the "Latitude Maxima" of the TIL can be used as a quantitative estimate of the changes in the TIL meridional structure over time, similar to other tropopause based metrics of the shift of the subtropical jet [*Seidel et al.*, 2008; *Davis and Rosenlof*, 2012]. UT TIL strength does not feature such sharp gradients (Figures 6d and 11d), so we will not focus on this metric in exploring changes in the subtropics.

Figure 12 illustrates trends in the peak latitude for five diagnostics in each hemisphere. Trends are estimated with the same bootstrap method by finding the peak in the zonal mean for each month, then calculating monthly anomalies (after removing the annual cycle). Annual anomalies yield similar quantitative trends. Both MERRA (gray) and ERAI (black) trends are shown in Figure 12. Error bars are the 95% confidence interval, so significant trends are where the error bars do not overlap the zero line. Figure 12 confirms the results in Figures 9 and 11. There are small shifts in the peak latitude of the N^2_{max} frequency and N^2_{max} separation from the tropopause (N2-Tp), with a tendency in ERAI to move equatorward (not seen in MERRA) Little change is seen in UT depth peaks in ERAI, while MERRA peaks move poleward. Both ERAI and MERRA indicate that the minimum subtropical LS depth and strength are moving poleward at $\sim$ 1° per decade. Southern Hemisphere trends are more coherent, and MERRA trends are smaller in the Northern Hemisphere.

4. Discussion/Conclusions

The TIL is well represented in ERAI and MERRA reanalyses relative to GPS soundings. The lower vertical resolution (and higher horizontal resolution) reanalysis can represent the TIL structure. We diagnose the TIL peak based on static stability (N^2_{max}). The peak is located above the tropopause. We also diagnose a "depth" and "strength" of the TIL on the stratospheric and tropospheric sides of this static stability peak. Results are consistent with previous work based on radiosondes [*Birner*, 2006] and GPS occultations [*Schmidt et al.*, 2010; *Grise et al.*, 2010].

There exists a coherent meridional structure to the TIL with a distinct difference between the tropics and extratropics. The subtropical TIL structure features a "tropopause break." In this region, the TIL is deeper

and has a minimum in strength on the stratospheric side. The TIL can be defined most (60–80%) of the time at any latitude. The TIL is not well defined around the subtropical jet and is also not present near strong tropopause height gradients, associated with UT synoptic systems (cutoff lows, Figure 3b) and strong PV gradients. The thermal structure profiles in these regions in the ERAI data often do not permit a TIL to be defined.

The TIL diagnostics show synoptic structure. TIL UT strength is anticorrelated to UT (500 hPa) PV: higher 500 hPa PV results in lower UT strength but tends toward greater UT TIL depth. UT TIL depth and strength are anticorrelated. UT TIL strength is low in cyclonic systems, consistent with previous analyses of TIL structure [*Homeyer et al.*, 2010] or as expected from balanced dynamics theory [*Wirth*, 2000, 2003] and observed with GPS data *Randel et al.* [2007b]. The LS is different. LS TIL depth and strength are positively correlated. The LS TIL depth responds to changes in the TIL peak. The correlation suggests that the LS TIL is governed by fluctuations near the tropopause (the lower bound of the LS TIL) and a large (and steady) background stability (PV) gradient in the lower stratosphere (the upper bound of the LS TIL).

What does this mean for transport? The TIL is a diagnostic of the dynamical structure of the UTLS. *Birner* [2006] pointed out the homogenization of PV on an isentropic surface co-located with the TIL. *Schmidt et al.* [2010] noted that the TIL contains the vertical gradient of trace gases like ozone and carbon monoxide. This indicates the TIL itself is co-located with the tropopause mixing layer [*Pan et al.*, 2007; *Kunz et al.*, 2009]. In addition, the presence and depth of the TIL sets the thickness of this region. Furthermore, the variability of the TIL structures in the subtropics is linked to the transport and layering of tropical and extratropical air. There is an anticorrelation between the UT and LS TIL depth: when the UT TIL is shallow, the LS tends to be deeper. This is not surprising as static stability is the vertical component of PV. The diagnostics of the TIL and the correspondence with the tropopause mixing layer mean that the TIL and the mixing layer may be diagnosed from static stability. As an example, the UT TIL depth and strength are anticorrelated in the seasonal cycle. The gradients between the tropics and extratropics in both the UT and LS are enhanced in winter, and the gradient spreads out in summer in both hemispheres. This is indicative of higher mixing in summer and has been seen in tracer observations [e.g., *Pan et al.*, 1997].

There are significant trends in the structure of the TIL. Over time, the UT TIL has appeared to thin at higher latitudes in the ERAI data by 5% per decade and the separation of N^2 and tropopause has decreased in the subtropics. In the LS, the TIL in the subtropics has gotten thicker and stronger. These trends are small but significant.

The trends manifest themselves also as a shift in the subtropical tropopause break, which appears in the ERAI and MERRA reanalyses to be moving poleward in the LS, while there are less robust trends for the UT diagnostics. The significant poleward trends in the LS minimum depth and strength are from 0.4° to 1.4° per decade in each hemisphere, broadly consistent with previous analyses of the trends in the subtropical tropopause break from observations or other measures of the change in tropical circulation [*Davis and Rosenlof*, 2012].

What do these trends mean? The TIL static stability gradient appears to be getting shallower and a little bit weaker in the UT. It seems likely that as the tropopause gets higher (lower pressure), the TIL is moving up, but also the gradients are tightening in space and weakening slightly. The LS TIL appears to be rising and strengthening above the tropical tropopause, as well as moving poleward. This is consistent with (a) changing temperatures of the tropical tropopause and cold point (though there is little observational evidence for this, it is predicted from model simulations with anthropogenic forcing) and (b) a complicated consequence of the shifting subtropical jets. Point (b) is a consequence of differential heating of the atmosphere induced by greenhouse gas forcing, which heats the TTL while having little effect on the extratropical LS between 10 and 16 km, increasing the thermal wind gradient and accelerating the jet, which then alters wave propagation and interactions with tropospheric waves, generally moving the jet poleward.

These TIL diagnostics will be a good test for global General Circulation Models (GCMs) to evaluate their TIL structure relative to the ERAI reanalysis and to also look at potential trends in historical hindcast forced simulations. These diagnostics would also allow an analysis of the future evolution of the TIL using future scenarios. This will be a subject for future work.

Acknowledgments
NCAR is sponsored by the U.S. National Science Foundation. This project started during a sabbatical at ETH Zurich and discussions with Heini Wernli. ERAI data were provided by Heini Wernli and MetoSwiss. Thanks to Peter Hoor and Thomas Birner for discussions. Thanks to Simone Tilmes for assistance with MERRA reanalysis and to Cameron Homeyer and Bill Randel for comments. ERAI data are available from ECMWF (http://www.ecmwf.int/research/era/do/get/era-interim). MERRA Reanalyses are available from NASA (http://gmao.gsfc.nasa.gov/merra/), and COSMIC GPS data are available from the University Corporation for Atmospheric Research (http://www.cosmic.ucar.edu/).

References

Anthes, R. A., et al. (2008), The COSMIC/FORMOSAT-3 mission: Early results, *Bull. Am. Meteorol. Soc.*, *89*, 313–333.
Birner, T. (2006), Fine-scale structure of the extratropical tropopause region, *J. Geophys. Res.*, *111*, D04104, doi:10.1029/2005JD006301.
Birner, T. (2010), Recent widening of the tropical belt from global tropopause statistics: Sensitivities, *J. Geophys. Res.*, *115*, D23109, doi:10.1029/2010JD014664.
Birner, T., A. Dornbrack, and U. Schumann (2002), How sharp is the tropopause at midlatitudes?, *Geophys. Res. Lett.*, *29*(14), 45-1–45-4, doi:10.1029/2002GL015142.
Birner, T., D. Sankey, and T. G. Shepherd (2006), The tropopause inversion layer in models and analyses, *Geophys. Res. Lett.*, *33*, L14804, doi:10.1029/2006GL026549.
Davis, N. A., and T. Birner (2013), Seasonal to multidecadal variability of the width of hte tropical belt, *J. Geophys. Res. Atmos.*, *118*, 7773–7787, doi:10.1002/jrgd.50610.
Davis, S. M., and K. H. Rosenlof (2012), A multidiagnostic intercomparison of tropical-width time series using reanalyses and satellite observations, *J. Clim.*, *25*, 1061–1078, doi:10.1175/JCLI-D-11-00127.1.
Dee, D. P., et al. (2011), The era-interim reanalysis: Configuration and performance of the data assimilation system, *Q. J. R. Meteorol. Soc.*, *137*(656), 553–597, doi:10.1002/qj.828.
Gettelman, A., et al. (2010), Multi-model assessment of the upper troposphere and lower stratosphere: Tropics and trends, *J. Geophys. Res.*, *115*, D00M08, doi:10.1029/2009JD013638.
Gettelman, A., P. Hoor, L. L. Pan, W. J. Randel, M. I. Hegglin, and T. Birner (2011), The extratropical upper troposphere and lower stratosphere, *Rev. Geophys.*, *49*, RG3003, doi:10.1029/2011RG000355.
Grise, K. M., D. W. J. Thompson, and T. Birner (2010), A global survey of static stability in the stratosphere and upper tropopshere, *J. Clim.*, *23*, 2275–2292.
Hegglin, M. I., C. D. Boone, G. L. Manney, and K. A. Walker (2009), A global view of the extratropical tropopause transition layer from Atmospheric Chemistry Experiment Fourier Transform Spectrometer O_3, H_2O, and CO, *J. Geophys. Res.*, *114*, D00B11, doi:10.1029/2008JD009984.
Held, I. M. (1982), On the height of the tropopause and the static stability of the troposphere, *J. Atmos. Sci.*, *39*, 412–417.
Held, I. M., and A. Y. Hou (1980), Nonlinear axially symmetric circulations in an almost inviscid atmosphere, *J. Atmos. Sci.*, *37*, 515–533.
Homeyer, C. R., K. P. Bowman, and L. L. Pan (2010), Extratropical tropopause transition layer characteristics from high resolution sounding data, *J. Geophys. Res.*, *115*, D13108, doi:10.1029/2009JD013664.
Kunz, A., P. Konopka, R. Müller, L. L. Pan, C. Schiller, and F. Rohrer (2009), High static stability in the mixing layer above the extratropical tropopause, *J. Geophys. Res.*, *114*, D16305, doi:10.1029/2009JD011840.
Lorenz, D. J., and E. T. DeWeaver (2007), Tropopause hieght and zonal wind response to global warming in the IPCC scenario integrations, *J. Geophys. Res.*, *112*, D10119, doi:10.1029/2006JD008087.
Lu, J., C. Deser, and T. Reichler (2009), Cause of the widening of the tropical belt since 1958, *Geophys. Res. Lett.*, *36*, L03803, doi:10.1029/2008GL036076.
Marquardt, C., and S. B. Healy (2005), Measurement noise and stratospheric gravity wave characteristics obtained from GPS occultation data, *J. Meteorol. Soc. Jpn.*, *83*(3), 417–428.
Pan, L., S. Solomon, W. Randel, J. F. Lamarque, P. Hess, J. Gille, E. W. Chiou, and M. P. McCormick (1997), Hemispheric asymmetries and seasonal variations of the lowermost stratospheric water vapor and ozone derived from SAGE II data, *J. Geophys. Res.*, *102*(D23), 28,177–28,184.
Pan, L. L., et al. (2007), Chemical behavior of the tropopause observed during the Stratosphere-Troposphere Analyses of Regional Transport experiment, *J. Geophys. Res.*, *112*, D18110, doi:10.1029/2007JD008645.
Polvani, L. M., and P. J. Kushner (2002), Tropospheric response to stratospheric perturbations in a relatively simple general circulation model, *Geophys. Res. Lett.*, *29*(7), 18-1–18-4, doi:10.1029/2001GL014284.
Randel, W. J., and F. Wu (2010), The polar summer tropopause inversion layer, *J. Atmos. Sci.*, *67*, 2572–2581, doi:10.1175/2010JAS3430.1.
Randel, W. J., D. J. Seidel, and L. L. Pan (2007a), Observational characteristics of double tropopauses, *J. Geophys. Res.*, *112*, D07309, doi:10.1029/2006JD007904.
Randel, W. J., F. Wu, and P. Forster (2007b), The extratropical tropopause inversion layer: Global observations with GPS data, and a radiative forcing mechanism, *J. Atmos. Sci.*, *64*, 4489–4496.
Rienecker, M. M., et al. (2011), MERRA: NASA's modern-era retrospective analysis for research and applications, *J. Clim.*, *24*, 3624–3648, doi:10.1175/JCLI-D-11-00015.1.
Schmidt, T., J.-P. Cammas, H. G. J. Smit, S. Heise, J. Wickert, and A. Hasler (2010), Observational characteristics of the tropopause inversion layer derived from CHAMP/GRACE radio occultations and MOZAIC aircraft data, *J. Geophys. Res.*, *115*, D24304, doi:10.1029/2010JD014284.
Seidel, D. J., Q. Fu, W. J. Randel, and T. Reichler (2008), Widening of the tropical belt in a changing climate, *Nat. Geosci.*, *1*, 21–24, doi:10.1038/ngeo.2007.38.
Son, S. W., and L. M. Polvani (2007), Dynamical formation of an extra-tropical tropopause inversion layer in a relatively simple general circulation model, *Geophys. Res. Lett.*, *34*, L17806, doi:10.1029/2007GL030564.
Wirth, V. (2000), Thermal versus dynamical tropopause in upper troposphere balanced flow anomalies, *Q. J. R. Meteorol. Soc.*, *126*, 299–317.
Wirth, V. (2001), Cyclone–anticyclone asymmetry concerning the height of the thermal and dynamical tropopause, *J. Atmos. Sci.*, *58*, 26–37.
Wirth, V. (2003), Static stability in the extratropical tropopause region, *J. Atmos. Sci.*, *60*, 1395–1409.
World Meteorological Organization (1957), Definition of the tropopause, *World Meteorol. Organ. Bull.*, *6*, 136.